Ann. Geophysicae 16: 492–509 (1998) © EGS – Springer-Verlag 1998

Annales Geophysicae

Long-term solar activity and terrestrial connections. Part II: at the beckon of the sun?

N. D. Diamantides

Department of Geography, Kent State University, P.O. Box 5190, Kent, Ohio 44242, USA

Received: 25 March 1996 / Revised: 16 August 1997 / Accepted: 5 September 1997

Abstract. The research task described herein aims at the structuring of an analytical tool that traces the time course of geophysical phenomena, regional or global, and compares it to the course of long-term solar conditions, long-term meaning decades or a few centuries. The model is based on the premise that since in a last analysis the preponderance of atmospheric, hydrospheric, and, possibly, some aspects of geospheric phenomena are, or have been, powered by energy issuing from the sun – either now or in the past – the long-term behavior of such phenomena is ultimately "connected" to long-term changes occurring in the sun itself. Accordingly, the proposed research firstly derives and models a stable *surrogate pattern* for the long-term solar activity, secondly introduces a *transfer-function* algorithm for modeling the connection between the surrogate and terrestrial phenomena viewed as partners in the connection, and thirdly probes the connection outcome for *episodic* or *unanticipated effects* that may arise due to the fact that in the present context, the connection, should it exist, is very likely nonlinear. Part I of the study presents the theory of the concept, while Part II demonstrates the concept's pertinence to a number of terrestrial phenomena.

Key words. Solar activity · Kolmogorov algorithm

1 Introduction

In Part I of this study (Diamantides, 1998) the presence of long-term patterning in solar activity was investigated and its macrodynamic features portrayed by means of a model describing the morphology of the process. In Part II which now follows, examples are presented demonstrating the pertinence of this formulation to terrestrial phenomena of considerable interest.

Although in a last analysis all such phenomena are powered either by energy stored in the earth's interior during its formation, or by energy issuing from the sun contemporarily, the physics of their relationship to the basic entity $z_{11}(t)$ of the present model, should it exist, is for the most part unknown. Therefore, the term *connection* will be used in examining possible relationships, the dictionary definition of the term 'connection' being: "Relation between things one of which is bound up with, or involved in, another" (The Shorter Oxford English Dictionary). Hence, in the present context, 'connection' neither implies a cause-effect relationship, nor excludes it; for all we know, both the solar and the terrestrial may be influenced by processes emanating from outside the solar/planetary system. In all cases examined subsequently, the long-term behavior of the phenomenon under scrutiny will be sought and, therefore, when necessary, data series given in terms of annual figures will be replaced by their 11-year average as defined by Eq. (7), Part I. Identification of the connection will then be searched by means of the transfer-function algorithm and/or the Kolmogorov algorithm, both of them employed in the realms of control-systems and communication-signals; with it, the presence of both harmonics and/or subharmonics of the 11-year sunspot cycle will be monitored in view of the basic tenet's corollary.

In what follows, a number of lithospheric and atmospheric phenomena are looked upon from this connection point of view. By analogy with the behavior of mechanical and/or electrical systems, each of the input agent's components: trend $T(t)$, surges $S_i(t)$ and time derivative $Dz_{11}(t)$ can be affecting the phenomenon under consideration differently. Therefore, to assess each component's relative contribution, the component's *normalized* counterpart will be entered into the presumed connection, the normalization algorithm being:

$$[f(t)] = (f(t) - f_{\text{avg}})/f_{\text{std}} \quad . \tag{1}$$

The terrestrial phenomena in Sects. 2–6 that follow are to be viewed in this light, their historical record, as well as that of $z_{11}(t)$, being given in the Appendices.

2 The Southern Oscillation Connection

The atmospheric circulation as well as the sea surface temperature, pressure, and subsurface currents in the western equatorial Pacific have exhibited remarkably consistent space and time patterns ever since their observation began in the middle of the last century. Several other atmospheric and oceanic features – both near to/and far from the site – vary in association with these patterns, including the very important *El Niño* phenomenon, and the climate dynamics of Oceania, Australia, New Zealand, and the western parts of the Americas (Phillander, 1992). The literature spurred by the phenomenon has been varied (Anderson and McTeay 1985; Cane *et al.*, 1986; Legrand and Simon, 1989; Quinn *et al.*, 1987; Simon and Legrand, 1989; Kerr, 1991; Simkin, 1994; Mendora *et al.*, 1991), often invoking the solar factor in various ways, like solar ultraviolet radiation, solar wind, general atmospheric circulation, ocean-atmosphere coupling, geomagnetic activity, solar winds, etc.

The phenomena and the physical mechanisms involved have been referred to as the *Southern Oscillation*. The importance of its influence upon global climate may be judged by the fact that 18 countries have invested in a decade of research named Tropical Ocean Global Atmosphere Study **(TOGA)** beginning with a search for temperature models of the tropical Pacific waters (Monastersky, 1993).

In this section of the study the 1850–1975 history of air barometric pressure over that area amassed by Wright (1977, 1995) is analyzed in the present context. The data has been arranged by Wright in a form which he named the *Southern Oscillation Index*, and which, arranged by season, is given in Appendix 1a,b. For our purposes the annual figures of the index for spring, i.e., March-April-May **(MAM)**; and fall, September-October-November **(SON)** will be combined to produce the function:

$$O(t) = (\mathrm{MAM} + \mathrm{SON})/2 \ , \tag{2}$$

and its long-term counterpart $O_{11}(t)$, both of which can be seen in Appendix 2 and Fig. 1. The reason for selecting Eq. (2) to represent the index is to track the average course of the Southern Oscillation phenomenon and avoid either one of the two extremes of winter (DJF) and summer (JJA) months. Beyond 1974 the index is extended to 1992 based on the difference $p(t)$ between the standardized sea-level pressure anomalies at Tahiti and Darwin (National Weather Service, 1992). The two records, having a common time-span in 1973–1994, make possible the expression of $O_{11}(t)$ as a linear function of $p(t)$ over this span, with the result being included in Appendix a and b. Then, in a trial step, $O_{11}(t)$ was set up as a linear function of the trend $T(t)$ and surge $S(t)$ components of $z_{11}(t)$, and the ensuing residual was probed for the presence of incommensurate frequencies: once again the second subharmonic of $z(t)$ was found in the residual's autocorrelogram leading to the final model:

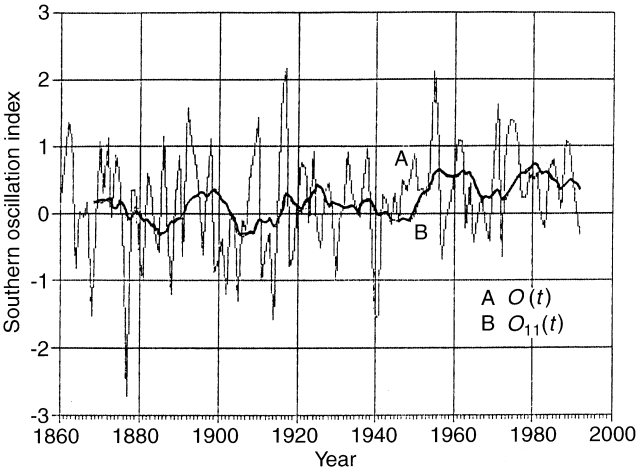

Fig. 1. Southern Oscillation (annual and long-term)

$$O_{11}(t) = a\,T(t) + b\,S(t) + m\,\sin(\tfrac{\omega}{2}t) + n\,\cos(\tfrac{\omega}{2}t) + c \ , \quad \omega = 2\pi/11 \ . \tag{3}$$

The resulting regression parameters are listed below:

	parameter	offset years i	$w(i)$
a	0.768 (0.161)	−20	+0.008
b	0.450 (0.084)	−16	−0.026
m	0.187 (0.098)	−12	−0.385
n	0.438 (0.090)	−8	−0.035
c	−0.364	−4	+0.443
R^2	0.665	$t_o = 1870$,	

normalizing constants

	O_{11}	$T(t)$	$S(t)$
avg	0.124	48.26	1.337
std	0.244	4.195	17.32

(4)

To the residual of this step, whose autocorrelation function is seen in Fig. 2, the Kolmogorov operation was applied resulting in the transfer function $w(i)$ also

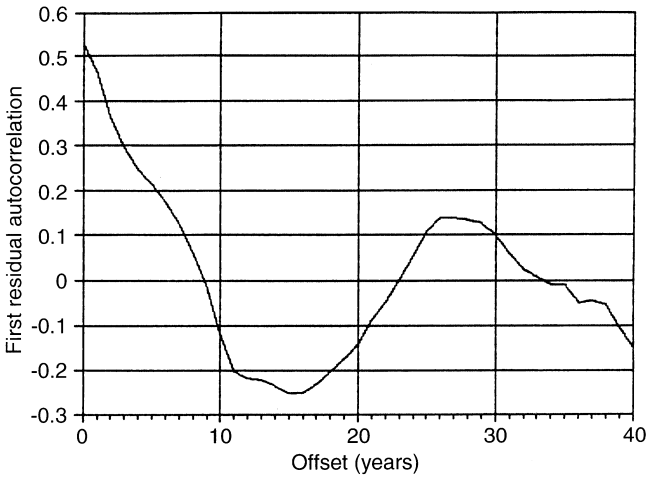

Fig. 2. Autocorrelation of first residual

shown in Eq. (4). The unit-time-step of 4 years was chosen because according to National Weather Service (1992) "the temporal behavior of the Southern Oscillation shows a quasi-periodicity of 3 to 5 years". The final residual proves definitely to be a random function, its autocorrelogram being the delta-function. Figure 3 of the final result shows how the solar 'connection', Eq. (3), and the ocean's surface thermodynamics presumably represented by the Kolmogorov sum, combine to power the phenomenon, with Fig. 4 showing the two components separately: their individual contributions to $O_{11}(t)$ as measured by their standard deviation (std) are 0.83 for the former and 0.45 for the latter. The model's adequacy may be judged by the fact that its standard deviation is 0.987 compared to 1 for the actual $O_{11}(t)$.

The outcome of this modeling therefore allays the hesitations expressed by, among others Enfield and Cid (1991), on the question of a solar connection presence. Finally, it should be pointed out that the presence of the sunspot number's period (11 years) has been noted in the analysis of climate behavior in an Atlantic Ocean counterpart of the Pacific Southern Oscillation; Ping *et al.* (1997) have proposed a model for the decadal variation of the sea surface temperature of the Atlantic north-south dipole. According to it, the variation is attributed to "an unstable thermodynamic ocean-atmosphere interaction between wind-induced heat fluxes and sea surface temperature". Under certain conditions, however, the model's so-called Dipole Index is an 11-year sinusoid (their Fig. 1b), and not the 10-year one they theorize, suggesting a solar connection.

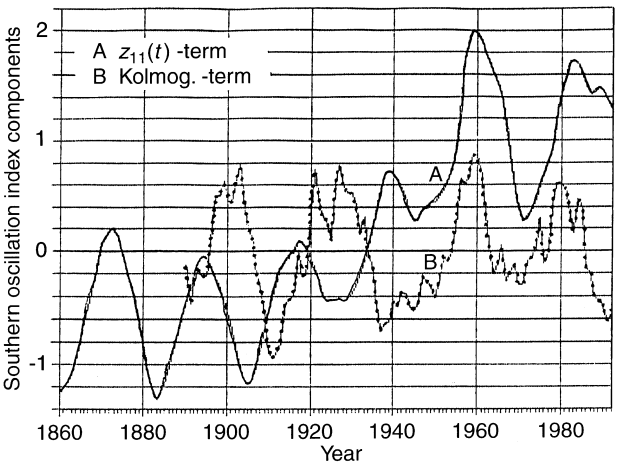

Fig. 4. Southern Oscillation components

3 The climatic connection

3.1 The atmospheric contaminants

The first climatic subject to be probed in the present context is the question of long-term changes in atmospheric gasses known to affect the radiative budget of the atmosphere; under the current state of the art, the most important of these atmospheric contaminants are carbon dioxide (CO_2) and the anthropogenic aerosols (Wigley and Raper, 1992), the growths of which have paralleled the growth of industrialization. For the purposes of this study, sulphur dioxide (SO_2) will be used as the surrogate of the influence of aerosols upon climate. The choice of these two agents reflects the fact that, while CO_2 constitutes a warming factor by being transparent to incoming visible radiation and opaque to outgoing infrared radiation, SO_2 can behave as a cooling factor most of the time, but not always, as explained later on. The 'contaminants' record, in parts per million by volume (ppmv), is given in Appendices 2 and 3.

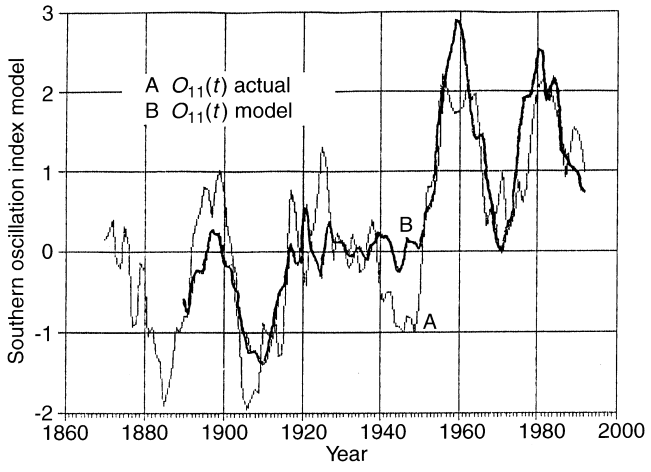

Fig. 3. Southern Oscillation model

3.1.1 The CO_2 factor. According to the researchers of the Physics Institute of the University of Bern (Neftel *et al.*, 1985), a detailed knowledge of the increase in CO_2 concentration since preindustrial times is a necessary prerequisite for understanding such aspects of the role of carbon dioxide as the sensitivity of climate to its concentration in the atmosphere and the contribution of biomass burning to the CO_2 increase. It is their view that the most reliable assessment of the ancient atmospheric CO_2 concentration is derived from measurements on the air occluded in ice cores. To this end, the researchers used a core from Siple Station in West Antarctica to determine the enclosed gas concentrations with a very good time resolution and over a time-span covering the last three centuries. The 200-m core was drilled in the summer of 1983–1984 by a team from the Bern Physics Institute and the Polar Ice Coring Office in Nebraska. The researchers' CO_2 concentration data from extracted air come from Table 1 and Fig. 1 of Naftel *et al.* (1985). It is reassuring to note that this record matches the one from a similar analysis of a core drilled in central Greenland by Wahlen *et al.* (1991). Here, the Siple Station data are the presumed output function $CO_2(t)$. The Naftel records were correlated with the trend component $T(t)$ of the long-term solar activity $z_{11}(t)$ of the present model over the period 1734–1940. The reason for this choice is the fact that the CO_2

record strongly suggests a low-pass filter characteristic for the presumed 'connection'. Accordingly, the simple functional relationship:

$$CO_2(t) = a\ T(t)^k \tag{5}$$

was subjected to linear regression over the 1745–1940 time-span, resulting in:

$$a = 98.626\ ,$$
$$k = 0.2834\ (0.0121)\ , \tag{6}$$
$$R^2 = 0.987\ .$$

As Fig. 5 shows, the agreement between the actual CO_2 data and the data from the model is remarkable up to about the year 1940, and so is the disagreement from that time on. The outcome is given in Table 1. According to it, the atmospheric CO_2 rate begins to outstrip that of $T(t)$ at about 1940, and this in spite of the fact that the $T(t)$ model used was the one with parameter values of Eq. (10) from Part I, making for a faster $T(t)$ rise than the constrain tenet allows. Quite obviously, the rapidity of this growth cannot all be attributed to the sun. The fact that the year 1940 marks the end of the worldwide depression of the 1930s and the onset of the most intensive and extensive industrial activity to date is very likely the reason. Equally important, however, is the fact that this manmade factor appears to have become aggravated by a nature-made positive feedback: recent studies (Prentice *et al.*, 1990; Oechel *et al.*, 1993; Smith and Shugart, 1993) have found that conditions have changed in the Arctic tundra, which during historic as well as recent geological times has been a net sink of CO_2 with large amounts of carbon being stored in the soils of northern ecosystems. But, with many regions of the Arctic becoming warmer than they were in the past, microbial action upon plant debris is enhanced, causing the soil to change from a sink to a source of CO_2. How much this affects the CO_2 budget is presently a matter of conjecture. In addition,

> regional effects can be much more variable – and uncertain – than global average projections. To this the nonlinear character of the system should be added, and the risks that nonlinearity often portends. (Ayres and Walter, 1991).

Table 1. CO_2 concentration (ppmv)

year	CO_2		year	CO_2	
	actual	model		actual	model
1785	279.5	277.5	1958	314.2	310.5
1805	280	280.8	1965	318	313.1
1825	284	283.7	1973	328	315.1
1853	288	289.3	1980		315.8
1873	292.3	293.1	1990		318.1
1894	297	297.3	2000		320.8
1914	300	301.5	2025		327.9
1932	306	305.4	2050		335.8
1949	311	309.2			

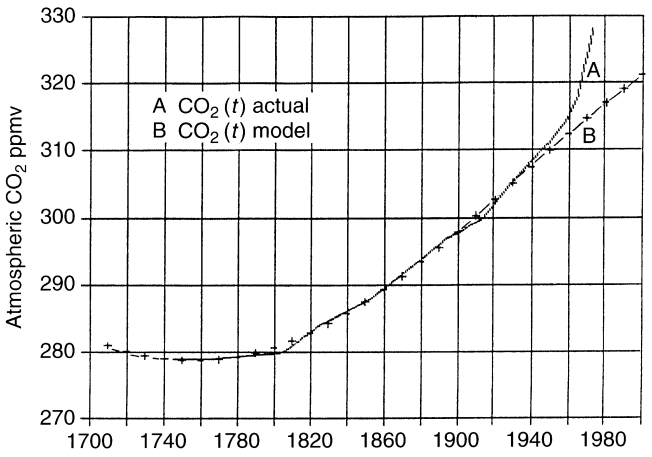

Fig. 5. Atmospheric CO_2

All these factors notwithstanding, should the relationship expressed by Eq. (5) hold into the distant future, a peaking of the atmospheric CO_2 content would occur at about the year 2050 at the level of 331.7 ppmv, if only solar influence were operative. Yet the level has already been reached at the beginning of the 1990s.

3.1.2 The SO_2 factor. The radiative forcing by atmospheric aerosols in general and by SO_2 in particular is quite involved. Radiative influences of aerosols on climate can be distinguished as direct, referring to the scattering and absorption of radiation by the aerosol particles themselves, and indirect, referring to the influence of aerosols on cloud formation (a complex process in itself), cloud lifetimes (Charlson *et al.*, 1992; Kellog, 1992; Lelieveld and Heintzenberg, 1992) and cloud altitude (tropospheric or lower-atmospheric). For all these reasons SO_2 climate forcing varies greatly with location and to the point where net warming instead of cooling may at times be the result. Anthropogenic aerosol emissions, primarily from fossil fuel combustion and metal smelting, have increased greatly over the industrial period (Charlson *et al.*, 1992). For this reason more than 90% of industrial SO_2 is emitted in the northern hemisphere, with the result that aerosol forcing is more of a factor there than in the southern hemisphere. By the same token, the forcing will be more pronounced in the industrial and large urban areas, and downwind from them than in open country. To this should be added the fact that radiation-related aerosol phenomena depend nonlinearly on aerosol concentration.

The time history of $SO_2(t)$, based on Moller (1984), is given in Appendix 3 – a history that is better appreciated through the function $\ln[SO_2(t)]$ shown in Fig. 6 (solid line). As seen there, $SO_2(t)$ has been growing steadily from 1800 to the present time at a rate only slightly affected by the Great Depression. Taking the optimistic stand that this growth rate cannot continue ad infinitum, let us use the notation:

$$y(t) = \ln[SO_2(t)]\ , \tag{7}$$

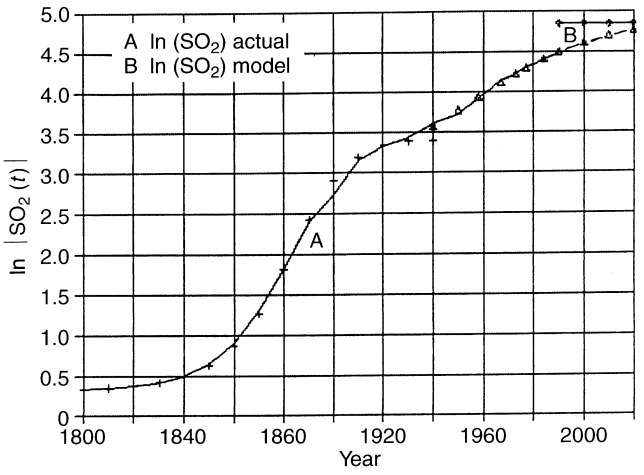

Fig. 6. Atmospheric SO_2

and resort to Eq. (2) of Part I to model the course of $y(t)$ in time. This allows the computation of the ln[SO_2]'s mediating factor $c(t)$:

$$C(t) = \int c(t)\mathrm{d}t = \ln \frac{1/y_{\min} - 1/y_{\max}}{1/y(t) - 1/y_{\max}} \quad , \tag{8}$$

assuming that $y_{\min}$ and $y_{\max}$ are found first. To this end, Eq. (4) of Part I applied to the ln[SO_2] data yields:

$$\begin{aligned} &1800-1820-1640 \quad \ln[SO_2]_{\min} = 0.323 \ (1.38 \text{ ppmv}) \\ &1890-1910-1940 \quad \ln[SO_2]_{\max} = 3.593 \ (36.35 \text{ ppmv}) \\ &1950-1967-1984 \quad \ln[SO_2]_{\max} = 4.842 \ (126.70 \text{ ppmv}) \ . \end{aligned} \tag{9}$$

Using a simple quadratic to model $C(t)$ we find:

$$C(t) = \exp(k_2(t-1800)^2 + k_1(t-1800) + k_0) \ ,$$

	1800–1940	1940–1990
k_2	$-0.261 \times 10^{-3}(0.212 \times 10^{-6})$	$0.226 \times 10^{-4}(0.964 \times 10^{-5})$
k_1	$-0.705 \times 10^{-1}(0.001)$	$-0.601 \times 10^{-3}(0.325 \times 10^{-3})$
k_0	-3.132	0.936
R^2	0.999	0.996

(10)

The outcome is shown in Table 2 and Fig. 6, indicating that, under the current rates of change of both the SO_2 emissions and the environmental legislation aiming at its control, the course of ln[SO_2] will hover around the 130-ppmv level.

3.2 The northern hemisphere temperature case

Recent homogenized near-surface temperature data over the land and oceans of both hemispheres have been combined by P.D. Jones and his team (Jones *et al.*, 1986) at East Anglia University to produce the first comprehensive estimates of the northern hemisphere's mean temperature $TH(t)$. His carefully scrutinized data

Table 2. SO_2 concentration (ppmv)

year	SO_2	year	SO_2	year	SO_2
1800	1.40	1890	9.3	1973	68.2
1810	1.42	1900	14.1	1977	74.9
1820	1.45	1910	21.3	1985	90
1830	1.51	1920	25	1990	93.3
1840	1.65	1930	27.1	2000	100
1850	1.92	1940	32.7	2010	101
1860	2.5	1950	36.8	2020	115
1870	3.9	1958	45.9	2030	119
1880	6.1	1967	56.5	2035	120

make possible the application of the present model to this extensive climatic measure. Table 3 gives summarily the $TH(t)$ record drawn from Appendix 4.

As seen in Fig. 7, hemispheric temperature advanced only little during the second half of the nineteenth century, increased markedly from 1910 to 1940, remained relatively steady in 1950–1975, and assumed a rapid track from then on. The variable on which this figure is based is the temperature anomaly above or below the 1950–1980 average.

Table 3. Northern hemisphere temperature

year	temp.	year	temp.	year	temp.
1860	−0.27	1905	− 0.25	1950	− 0.14
1865	−0.10	1910	− 0.31	1955	− 0.11
1870	−0.18	1915	+0.04	1960	+0.06
1875	−0.33	1920	− 0.14	1965	− 0.14
1880	−0.18	1925	− 0.10	1970	+0.01
1885	−0.26	1930	− 0.05	1975	− 0.07
1890	−0.25	1935	− 0.05	1980	+0.16
1895	−0.25	1940	+0.14	1985	+0.07
1900	−0.01	1945	+0.09	1989	+0.23

Our modeling of $TH(t)$ was done in two steps: in the first, the long-term temperature function $TH_{11}(t)$ was generated based on the 1855–1989 data:

$$TH_{11}(t) = \frac{1}{11} \sum_{1}^{11} TH(t) \ , \tag{11}$$

and was set as the supposed effect of z_{11} CO_2, and SO_2; linear regression then showed the contribution by $z_{11}(t)$ to be hardly distinguishable from noise, but revealed the presence of two incommensurate frequencies (22 years, and 80 years the Gleissberg cycle) calling for a model:

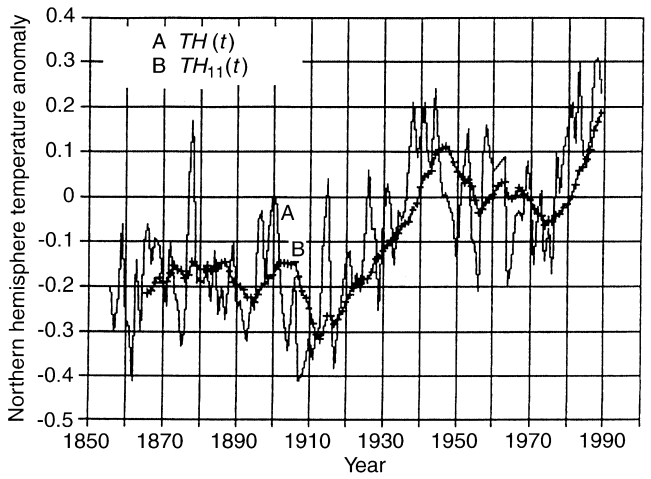

Fig. 7. Northern hemisphere temperature anomaly

$$\overline{TH}_{11}(t) = a\ \mathrm{CO}_{2,11}(t) + b\ \mathrm{SO}_{2,11}(t) + \sum_i \left[m_1 \sin\left(\frac{2\pi}{i}t\right) + n_1\left(\frac{2\pi}{i}t_y\right)\right] + c, \quad (12)$$

$$i = 22,\ 80 \qquad t \geq 1880,$$

with the constants of the new regression as follows:

			j years	$w(j)$
a	$+0.01387$	(0.00163)	-11	$+0.1094$
b	-0.00310	(0.00007)	-9	-0.1476
m_1	-0.01037	(0.00515)	-7	-0.0029
m_2	$+0.09203$	(0.09499)	-5	-0.0466
n_1	$+0.00550$	(0.00489)	-3	$+0.0062$
n_2	-0.03411	(0.00485)	-1	$+0.9641$
	c	-4.233		
	R^2	0.906 .		

(13)

It is interesting to note that the algebraic signs of the regression parameters show CO_2 to be a warming agent, and SO_2 a cooling one.

The regression residual $r(t)$, shown in Fig. 8 as curve C (std = 0.0334), were subjected to the Kolmogorov algorithm, producing the transfer function $w(i)$ that is included in the foregoing tabulation. Thus, the final model is:

$$\overline{TH}_{11}(t) = a\ \mathrm{CO}_{2,11}(t) + b\ \mathrm{SO}_{2,11}(t) + r(t) + \sum_i \left[m_1 \sin\left(\frac{2\pi}{i}t\right) + n_1\left(\frac{2\pi}{i}t\right)\right] + c + r(t)\ , \quad (14)$$

The latter is shown as curve B in the figure, and the final residual as curve D (std = 0.0126). Finally, curve E singles out the anthropogenic factor:

$$a\mathrm{CO}_{2,11}(t) + b\mathrm{SO}_{2,11}(t) + c\ , \quad (15)$$

showing it to be taking off at a steep rate from the 1970s on.

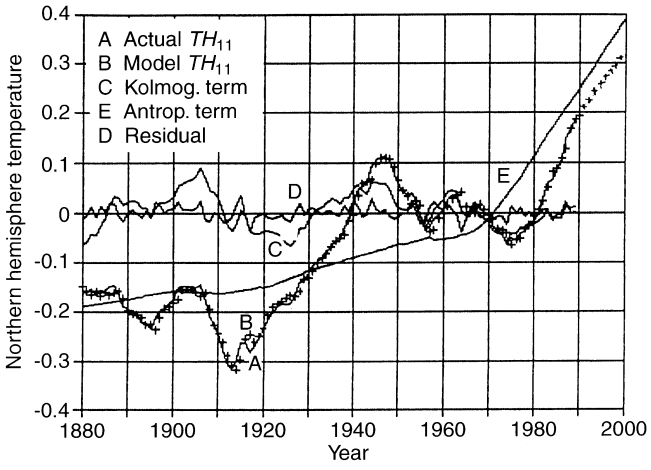

Fig. 8. Northern hemisphere temperature anomaly model

4 The seismic connection

The possibility of extraterrestrial (planetary) connection for terrestrial seismism has been considered by research workers in the past (Gribbin and Plagemann, 1974; Lomnitz, 1994) by invoking the combined gravity attraction of the sun's planetary system on the lithosphere as the quake trigger mechanism. It is of course a straightforward matter to compute the intensity of this force by applying Newton's equation of gravity and, through it, obtain the fluctuations of the force over the 1700–2100 span. The outcome is a regularly fluctuating function of time with peaks about 10 years apart, a regularity not found in the seismic record and, therefore, not supporting the planetary connection view.

The possibility of a relationship between earthquakes and solar activity per se has been discussed previously by various authors (Sytinski, 1963; Simpson, 1967; Singh, 1976). Simpson, for example, used the sunspot numbers, and the solar radioflux in combination with geomagnetic activity as indicators, and concluded that a significant role is played by solar activity in the triggering of earthquakes. Singh opines that whatever mechanism of energy-coupling seems to be working, the magnitude of such energy seems to be very small and, therefore, any contribution of the solar activity to seismic events should be more pronounced and more easily discernible in the case of very small energy seismic events, called microearthquakes. He then proceeds to conduct a small experimental research which leads him to conclude "that the solar activity is by no means an exclusive factor in the timing of microearthquakes". In what follows, the case of severe earthquakes is investigated. For this, the question of a solar 'connection' will be probed using actual quake data for which the case of the California area (CA) is particularly interesting; it accounts for more than eighty percent of all seismic activity in the contiguous United States.

Exact countrywide seismological information amassed in a systematic and consistent way has been available in the United States only from the beginning of the current century; this is because of the fact that in the

early days much of the country was sparsely settled and seismographic stations relatively few or nonexistent.

We may begin by setting up, for a particular territory and year t, an *annual index of seismicity* $Q(t)$ defined as the sum of the year's n quakes whose magnitudes are $q_i > 5$, or intensities $q_i >$ VI):

$$Q(t) = \sum_{1}^{n} q_i, \qquad q_i > 5 \text{ or VI}. \tag{16}$$

From this, the long-term seismicity index is derived as

$$Q_{11}(t) = \frac{1}{11} \sum_{t-10}^{t} Q(t) \ . \tag{17}$$

The quake magnitude limit of 5 units set for Eq. (16) reflects the fact that small (unbounded) earthquakes triggered within the seismogenic zone of the earth's crust exhibit frequency/magnitude distributions different from those of large (bounded) earthquakes occurring past the down-dip width of that zone (Pachaco *et al.*, 1992). It is the second kind of disturbance that the lower magnitude limit of 5 singles out. While the plate-tectonics phenomena causing the occurrence of an earthquake in a given locale are today fairly well understood, very little is known about any patterning in their timing and frequency of occurrence. In the context of the present search, we may check for one in a solar 'connection':

$$\overline{Q}_{11}(t) = f[z_{11}(t)] \ . \tag{18}$$

For the California area the U.S. Government Reports cited in the references contain all the factual information presently known about the subject, excluding the mathematics of its physical mechanism. They include tabular listing of earthquake date, location, magnitude, and intensity. To quote from that source:

> *magnitude* is a logarithmic measure of the energy released as seismic waves at the focus of an earthquake. Although such a scale has neither "top" nor "bottom" values, the highest earthquake magnitude known to have been calculated is about 9.5 units on a Richter scale and the lowest about −3.0. On the other hand, the term *intensity* represents a measure assigned subjectively based on a quake's effects upon: (1) people (i.e., the number of persons noticing, affected, frightened, panicked, etc), (2) effects on manmade structures (chimneys, walls, etc), and (3) effects on the Earth's surface (landslides, faultings, etc). Intensity therefore is more of a *subjective* tool resorted to when lack of instrumentation prevents the objective magnitude computation. The quantitative relationship between the two measures has been computed based on quake cases where both were available.

Because in the data sources used magnitudes are very often given in differing scales (M_L, M_s, M_{La}, M_{Ls}), or are unavailable while intensities are, the latter will be used in our analysis and introduced in the equations not as Roman numerals but as their decimal equivalents. For the western United States, where the CA area lies, the suggested magnitude/intensity relationship (U.S. Government, item 1, p. 4) is given in the tabulation below:

intensity	magnitude	intensity	magnitude
V	< 5.0	IX	6.5
VI	5.0	X	7.0
VII	5.5	XI	7.5
VIII	6.0	XII	8.0 .

Appendix 5 contains the $Q(t)$ data (in intensity units), while both $Q(t)$ and $Q_{11}(t)$ over the 1880–1989 period are seen in Fig. 9. Using this record $Q_{11}(t)$ was set as the simplest form of Eq. (18), namely:

$$\overline{Q}_{11}(t) = a\, z_{11}(t) + c \ ; \tag{19}$$

application of linear regression and probing its residual suggested the presence of the second subharmonic of the sunspot number $z(t)$. Hence, the processes were repeated using:

$$\overline{Q}_{11}(t) = a\, z_{11}(t) + m_1 \ \sin\left(\frac{2\pi}{22}t\right) + m_2 \ \cos\left(\frac{2\pi}{22}t\right) + c \ . \tag{20}$$

The residual of this regression in turn revealed a definite patterning $p(t)$ with a 50-year repetition rate, which after a moderated filtering:

$$\overline{p}(t) = 0.25p(t-1) + 0,50p(t) + 0.25p(t+1) \ , \tag{21}$$

is listed in Table 4 and pictured in Fig. 10; this term added to the right-hand member of Eq. (20) as $bp(t)$, contributed to the model regression as seen by:

$$\begin{aligned} &a = 0.659 \quad (0.015), \\ &b = 1.074 \quad (0.071), \\ &m_1 = 1.643 \quad (0.435), \\ &m_2 = 3.706 \quad (0.431), \\ &c = -7.859, \\ &R^2 = 0.960, \qquad t_0 = 1890 \ . \end{aligned} \tag{22}$$

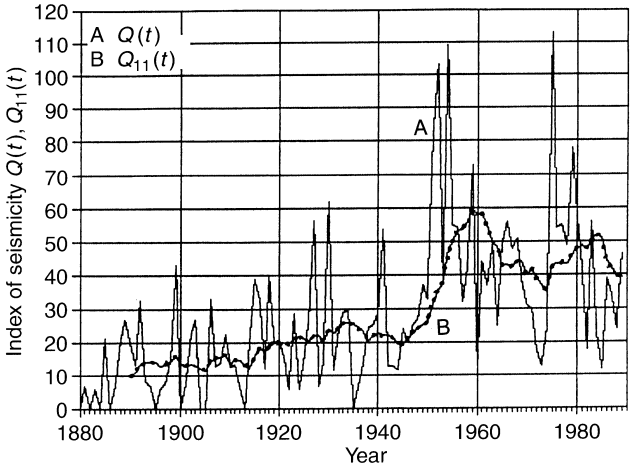

Fig. 9. California seismicity index

Table 4. Patterned residual of model $Q_{11}(t)$

year	$\overline{p}(t)$	year	$\overline{p}(t)$	year	$\overline{p}(t)$	year	$\overline{p}(t)$	year	$\overline{p}(t)$
1940	−6.3	1950	−6.8	1960	0.2	1970	5.4	1980	2.3
1941	−7.1	1951	−6.4	1961	0.3	1971	7.1	1981	2.4
1942	−6.3	1952	−5.3	1962	0.2	1972	7.0	1982	1.9
1943	−5.5	1953	−3.8	1963	−0.3	1973	6.3	1983	2.9
1944	−5.0	1954	−0.8	1964	−1.0	1974	4.5	1984	4.0
1945	−5.2	1955	2.1	1965	−2.6	1975	4.5	1985	5.8
1946	−5.7	1956	3.4	1966	−2.8	1976	4.5	1986	5.4
1947	−6.4	1957	2.5	1967	−1.5	1977	4.4	1987	3.8
1948	−6.8	1958	0.9	1968	0.9	1978	3.4	1988	0.2
1949	−7.2	1959	0.5	1969	3.8	1979	2.9	1989	−3.5

Figure. 10 shows $\overline{p}(t)$ superimposed upon the original $p(t)$ from which it was derived. It also shows $Q_{11}(t)$ and its model counterpart $\overline{Q}_{11}(t)$ supporting the assumption of solar connection, albeit lacking the identification of $p(t)$. The present state of the art in understanding the mechanics of the stick-and-slip process taking place at the boundary between the North American and Eastern Pacific tectonic plates on which California lies is part of the problem (Zielinski *et al.*, 1994). In the mean time, the autocorrelogram of the residual of the preceding regression, seen in Fig. 11 reveals the presence of the 8-year periodicity found in $Dz_{11}(t)$, Eq. (52) Part I. This provides the means of projecting $p(t)$, which, along with the projection of $z_{11}(t)$ also found in Part I, make possible a good estimate of $Q_{11}(t)$ during the 1995–2005 span seen in Fig. 12. It points to a moderate upswing in the mid-1990s, to be followed by a period of subsiding seismic activity.

Besides the seismicity index, a separate modeling of the series of the annual strongest quake $q_{\max}(t)$ would have been of value; but, unfortunately, no deterministic measure can be found in the data. Instead, the distribution $P[q_{\max}]$ of the 1880–1990 period may be seen in Fig. 13 and in Table 5, with the most probable maximum value being 5.5 Richter units. The expected upper and lower probability limits for the frequency distribution of quake magnitudes 5 or greater were derived by fitting a separate decaying exponential through the

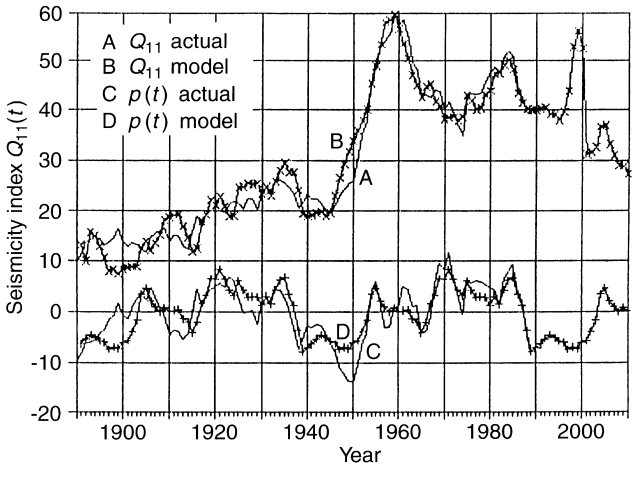

Fig. 10. Seismicity index model and residual

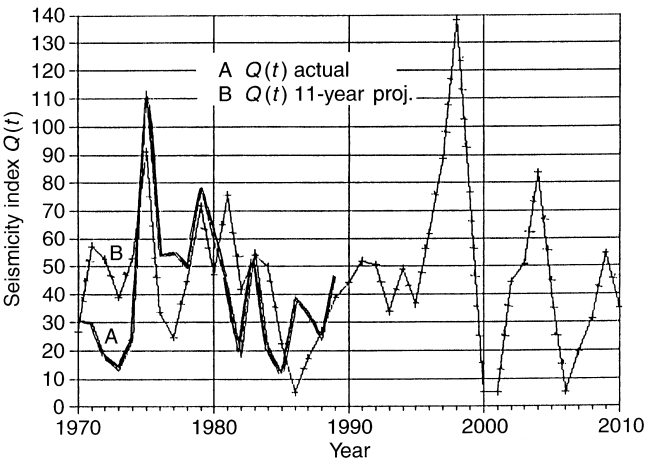

Fig. 11. Seismicity index projection

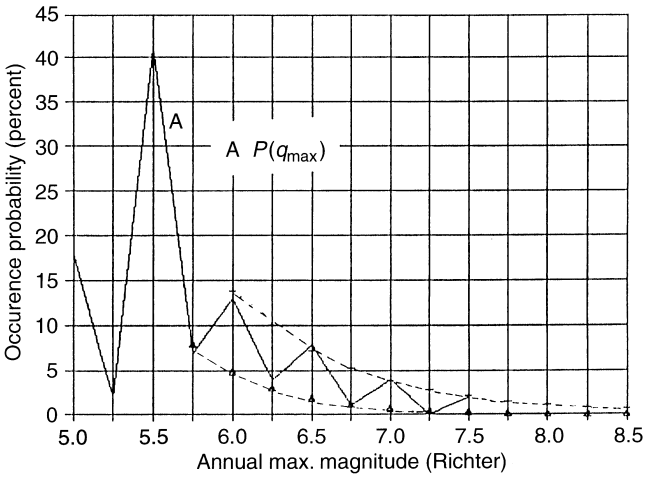

Fig. 12. Distribution of annual max. quake

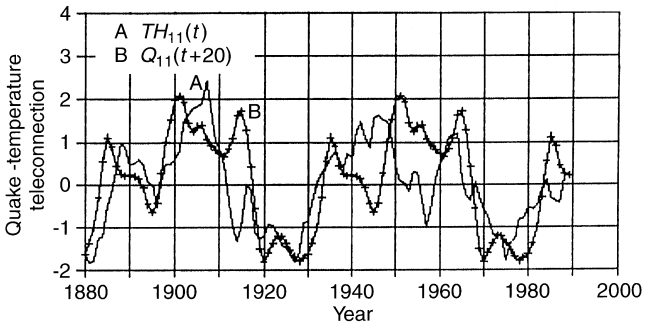

Fig. 13. Quake-temperature teleconnection

peaks and valleys of the $P[q_{\max}]$ data ($R^2 = 0.99$ for the peaks and 0.94 for the valleys).

Of interest in terms of teleconnection is the similarity of time paths between the $\overline{p}(t)$ factor of the California earthquakes $Q_{11}(t)$ and the Kolmogorov term of the northern hemisphere temperature $TH_{11}(t-20)$, 20 years earlier, both of them normalized. It is shown in Fig. 13, after $TH_{11}(t)$'s Kolmogorov part was subjected to the same moderate smoothing:

Table 5. distribution $P[q_{\max}]$

$q_{\max}$ intens.	magn.	$P[q_{\max}]$ %	limits % lower	upper
VI	5	18	–	–
	5.25	2	–	–
VII	5.5	41	–	–
	5.75	7	–	–
VIII	6	13	4.9	13.8
	6.25	4	3.0	10.1
IX	6.5	8	1.9	7.4
	6.75	1	1.1	5.4
X	7	4	0.7	3.9
	7.25	0	0.4	2.9
XI	7.5	2	0.3	2.1
	7.75		0.2	1.5
XII	8		0.1	1.1
	8.25		0.1	0.8
XIII	8.5		0.05	0.5

$$\overline{y}(t) = 0.25\ y(t-1) + 0.5\ y(t) + 0.25\ y(t+1) \qquad (24)$$

that had been applied to $p(t)$.

5 The volcanic connection

Volcanic activity throughout the globe is the result of crustal thermal and mechanical changes powered by the energy stored in the planet's core. However, important as volcanism is, its record is fragmentary, uncertain, and scattered, in spite of the fact that volcanos provide some of the most awesome and spectacular examples of natural change on earth. References (Simkin *et al.*, 1981) and (McClelland *et al.*, 1989) are the main source of data presently available. Besides eruption time and duration from which the number $N(t)$ of active volcanos during a given year t is determined, these two sources also give the so-called *Explosivity Index* through which the magnitude of each eruption is quantified. This measure

> combines total volume of products, descriptive terms of deposits, eruptive cloud height, and other measures, to yield a simple 0-to-8 index of increasing explosivity. However, the reported size, or bigness, of historic eruptions depends very much on the experience and vantage point of the observer. It is easy, therefore, to understand why one observer's 'major' eruption might be another's 'moderate', or even 'small' event (Simkin *et al.*, 1981, p. 20)

For the purposes of the present research therefore, not the ambiguous explosivity index but the number of yearly explosions $N(t)$ will be used, corrected on the basis of the so-called *Reporting Index* (Simkin *et al.*, 1981, p. 23) which we may designate by $R(t)$. The index is defined as the number of volcanos active during a given decade as a percentage of the number of volcanos known at the start of the decade. As shown in Fig. 14, line A (replicated from Simkin *et al.*, 1981) the time history of volcanism over the last 600 years exhibits three plateaux, of which the last one (1838–present) is virtually a constant $r(t) = 33$ and is preceded by a practically linear transitory phase, line B, with the year 1622 being the line's time-axis intercept. Thus, the time-function for $R(t)$ will be:

$$R(t) = -\begin{cases} 0.141\ (t - 1622), & 1622 \le t \le 1838, \\ 33\ , & t > 1838. \end{cases} \qquad (25)$$

Hence, the surrogate of volcanic activity on the basis of which the possibility of a solar 'connection' will be explored is the quantity:

$$V(t) = \frac{N(t)}{R(t)}, \qquad t \ge 1800\ , \qquad (26)$$

which we choose to name the *Index of Volcanism*. Appendix 6 lists the $V(t)$ series. Following Simkin's lead, a long-term average of $V(t)$ will be examined as the representative of the case: as such we choose the 11-year running average V_{11} and its rate of change DV_{11}:

$$V_{11}(t) = \frac{1}{11}\sum_{i}^{11} V(i), \qquad DV_{11}(t) = V_{11}(t) - V_{11}(t-1)\ . \qquad (27)$$

Figure 15 shows the course of the index since 1800.

Since at the present time no clues exist in the literature as to possible long-term time patterns for

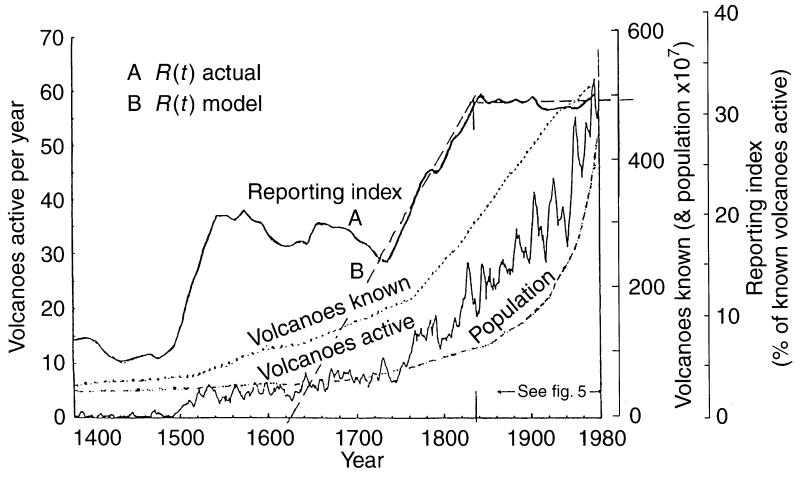

Fig. 14. Active-volcanoans and reporting index

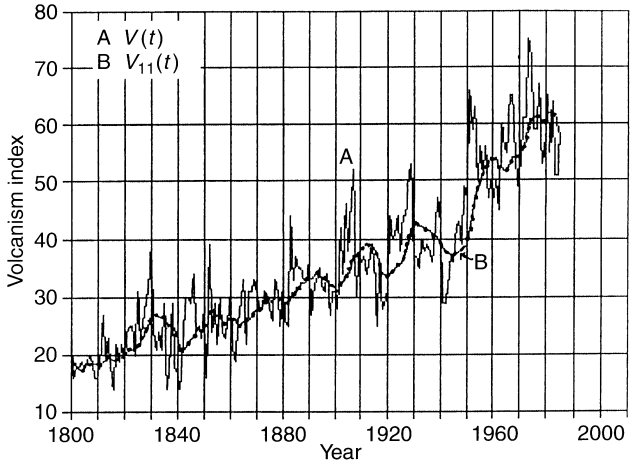

Fig. 15. Global volcanism (annual and long-term)

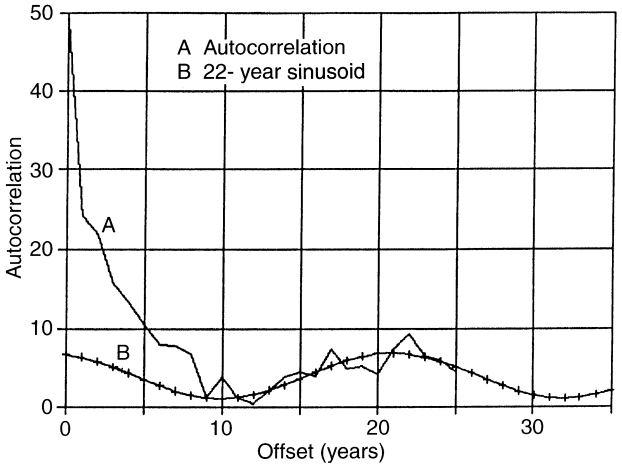

Fig. 16. Volcanism and "groomed" solar signal 1

$V_{11}(t)$, our search began by first making the secular trend $TV(t)$ of $V_{11}(t)$ function of the long-term $Tz(t)$ of $z_{11}(t)$ (see Part I):

$$TV(t) = a\ Tz(t)^k,$$

$$a = 0.000089$$
$$k = 3.3092\ (0.0693) \qquad (28)$$
$$R^2 = 0.945$$

$$1800 \leq t \leq 1985\ .$$

Since in Part I it was found that $Tz(t)$ peaks in the year 2100 at the level $Tz_{\max} = 60.8$, it follows that

$$TV_{\max} = a(Tz_{\max})^k = 65.0\ . \qquad (29)$$

On the other hand, to find $TV_{\min}$, the quadratic approximation was used over the 1800–1885 span of $V_{11}(t)$ yielding an $R^2 = 0.915$ and

$$TV_{\min} = 19.1\ . \qquad (30)$$

With the upper and lower limits of $TV(t)$ now known, use of Eq. (2), Part I, can be tried in search of a V_{11} versus $z_{11}(t)$ connection. From that equation one derives:

$$C(t) = \ln \frac{1/TV_{\min} - 1/TV_{\max}}{1/V_{11}(t) - 1/TV_{\max}}\ , \qquad (31)$$

where

$$C(t) = c(t)\mathrm{d}t\ ,$$

and therefore

$$c(t) = C(t) - C(t-1)\ . \qquad (32)$$

Subjecting $V_{11}(t) - TV_{11}(t)$ to the autocorrelation operation yields the function shown in Fig. 16, which reveals two things:

1. a strong delta-function representing a random component,
2. a component with a periodicity of 22 years, suggesting again the periodicity of the polarity of the magnetic field in the sunspot number $z(t)$.

By multiplying the $z(t)$ values of every other $z(t)$ cycle by -1 and naming the new series $zz(t)$, the polarity factor was incorporated in the sunspot series. Comparison of $c(t)$ to $DV_{11}(t)$, as seen in Fig. 17, shows a marked agreement between the two, but two differences:

1. an 11-year fixed time-delay of DV_{11} behind $zz(t)$ over the interval 1825–1883, which is roughly that of the upper part of surge S_{xx},
2. a 5.5-year fixed time-delay of DV_{11} behind $zz(t)$ from the year 1936 on, which is the beginning of the upper part of surge S_{xxx}.

By upper part we mean the positive segment of the normalized surge function S_{xx} or S_{xxx}.

Figure 18 shows the extent of the agreement after these time-lags were incorporated in $zz(t)$, changing it to $\overline{zz}(t)$. For lack of a better term, we are going to refer to $\overline{zz}(t)$ from now on as the '*groomed*' $zz(t)$. The high degree of coherence between the solar and the volcanic is best demonstrated by the two curves in Fig. 19, of which A is the autocorrelogram of $\overline{zz}(t)$ and B the cross-correlogram of $zz(t)$ with $\overline{DV}_{11}(t)$. Both correlations were computed over the 1800–1985 time-span. Under these circumstances the possibility of a solar-terrestrial

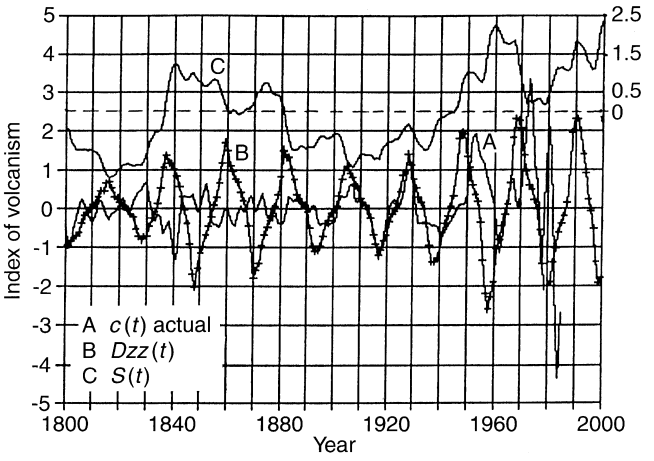

Fig. 17. Volcanism and "groomed" solar signal 2

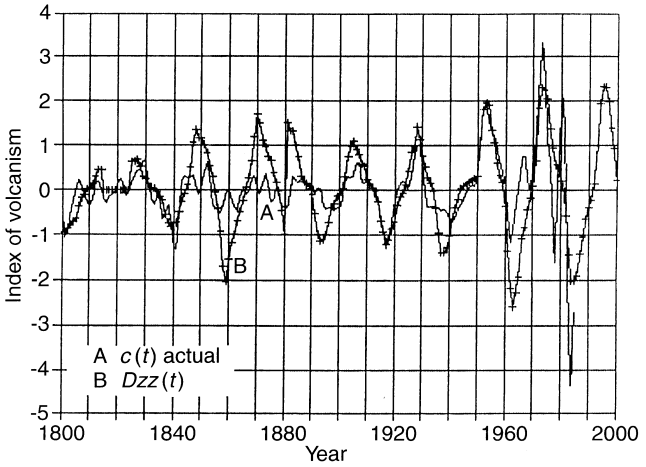

Fig. 18. Volcanism and "groomed" solar signal 3

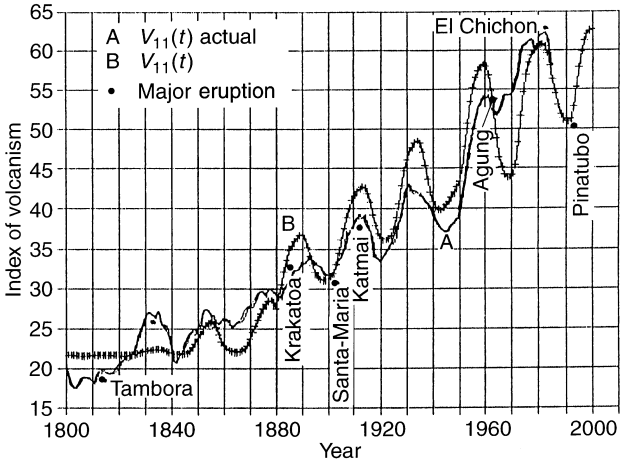

Fig. 20. Global volcanism and major eruptions

'connection' in this case cannot be ruled out. The two nonlinearities were brought to bear upon $C(t)$ in the following manner:

$$C(t) = a|Dzz(t)|^m \,*\text{sign}\, |Dzz(t)| + b\, Dzz(t) + c \ , \qquad (33)$$

for which iterative linear regression produced:

$$\begin{aligned} a &= 0.218 \quad (0.017), \\ b &= -0.040 \quad (0.039), \\ c &= 0.144, \\ m &= 2, \\ R^2 &= 0.898 \ . \end{aligned} \qquad (34)$$

The outcome is pictured in Fig. 20, foretelling the relative volcanic activity quiescence of the early-to-mid 1990s and a new upswing as the year 2000 approaches.

Two points of interest emerge from this analysis: first, the time-delay between the terrestrial and the solar occurring at the peaking of the long-term solar activity; and second, the fact that of the eight most violent eruptions of the last two hundred years (Angel and Korshover, 1985; Zielinski *et al.*, 1994):

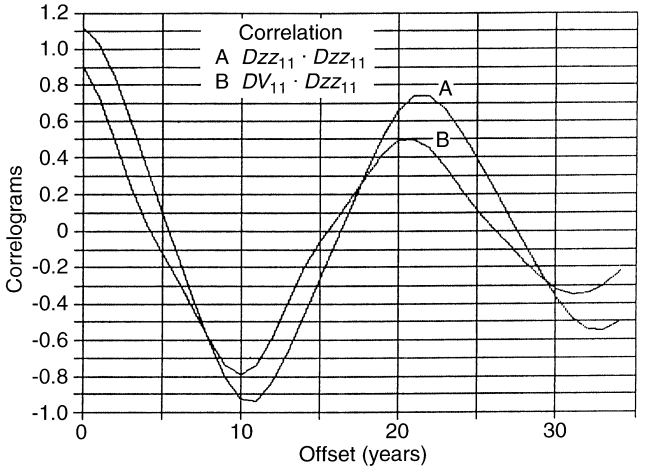

Fig. 19. Volcanic and solar cross-correlations

Tambora 1815
Coseguina 1835
Krakatoa 1883
Santa Maria 1902
Katmai 1912
Agung 1963
El Chichon 1982
Pinatubo 1991

four occurred at the very bottom of the V_{11} undulations, and three at a peak.

6 A tree-ring connection

Tree-ring research has a long and extensive tradition in physical science, and a wealth of findings revealing details of past climates over far-flung parts of the world. The Laboratory of Tree-Ring Research of the University of Arizona at Tucson clearly stands out in this realm of scientific research. Of the voluminous record of studies compiled there, and elsewhere, we choose to present one that strongly suggests a long-term connection between things terrestrial and solar, and this over the last three centuries. According to Lamb (1973, p 449), a general turn toward colder climates from 1200–1400 AD onward seems to have produced a worldwide cold stage lasting well into the 17th century. This stage was widely known in Europe of the late Middle Ages as the climatic worsening (Klima-Verschlechterung). Tree growth, and therefore tree-ring record, seems to bear witness to this cooling and to the recovery that followed it, beginning with the early 1700s.

There are many studies documenting the fact that, in addition to climate, tree-ring growth is very much dependent on local conditions of soil composition, human activity interference, and the prevailing atmospheric composition (see for instance, McLaughlin and Tjoelker, 1992, 1993; McLaughlin *et al.*, 1994; McLaughlin and Downing, 1995; also, Francey and Farquhar 1982; Andersen *et al.*, 1991). Consequently, data normalization is necessary when comparing cases. In what follows, the data of two sets of oak-tree ring

measurements are grouped into one body of data in order to widen the time-span covered, namely: (1) in a study by Hollstein (1965) tree-ring widths of oak west of the Rhine near Trier, 1350–1700, were measured; (2) in a study by Libby and Pandolti (1974) the anomaly of the oxygen isotope ratio $^{18}O/^{16}O$ was measured in the tree-ring dated wood of oak trees in two areas of Germany, Marburg (five trees) and Spessart (two trees), and a 30-year running average was computed over the 1750–1960 time-interval. Each set of data was normalized to its own average and standard deviation, and the composite tree-ring set $TR(t)$, seen in Table 6 and Fig. 21, was structured from (1) the Rhine data over 1350–1700, (2) the (Rhine + Marburg)/2 data over 1700–1750, and (3) the Marburg data over 1750–1960. Included for comparison in this figure is the normalized $z_{11}(t)$ curve. It is interesting to note that $z_{11}(t)$ is shown *lagging* behind $TR(t)$, a fact confirmed by Fig. 22, which pictures the correlation functions $TR * TR$ and $TR * z_{11}$, and pinpoints the length of the lag to between 30 and 40 years. The explanation for this lag is found in Eddy (1976), based on the past abundance of terrestrial ^{14}C: carbon and its radioactive isotopes are abundant constituents of the earth's atmosphere as CO_2; given that when the latter is assimilated into trees the carbon isotope ^{14}C undergoes spontaneous disintegration at well-known rates, it is possible to determine the date of life of the carbon-bearing tree wood. Thus, the ^{14}C curve is a fair representation of the overall envelope of the sunspot curve and of real changes in solar behavior in the distant past before the time of telescopic examination of the sun. According to Eddy (1976, p. 1896):

> the ^{14}C indications will tend to lag behind the real solar changes by periods of 10 to 50 years, because of the finite time of exchange between the atmosphere and the trees.

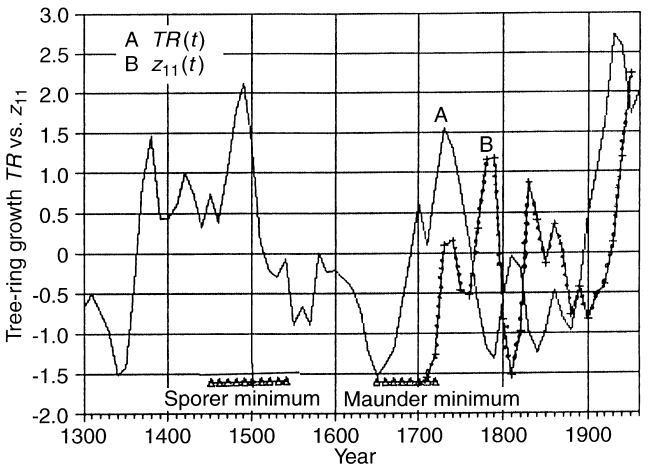

Fig. 21. Long-term tree-rings and solar activity

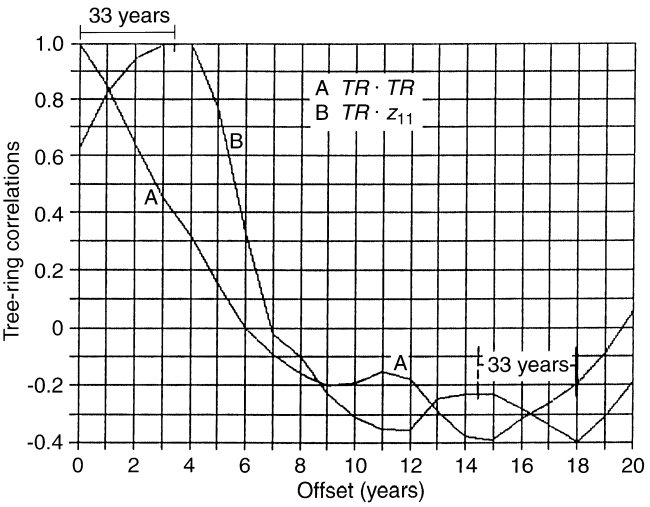

Fig. 22. Tree-ring/solar-activity cross-correlations

Table 6. Tree-ring data

year	Rhine	German	year	Rhine	German	year	Rhine	German
1350	95.3	–	1560	104.7	1.35	1770	130	0.84
1360	108.7	–	1570	102	1.6	1780	125.7	0.45
1370	123.3	1.49	1580	113	1.7	1790	127.7	0.35
1380	131	1.55	1590	110	1.26	1800	118.7	0.9
1390	118.3	1.56	1600	110.3	1.061	1810	117	1.25
1400	118.3	1.5	1610	109	1.05	1820	111.3	1.15
1410	120.3	1.6	1620	107.7	1.2	1830	110	0.6
1420	125.3	1.54	1630	104	1.3	1840	107	0.4
1430	122	1.49	1640	97.7	1.4	1850	102	0.6
1440	117	1.4	1650	94	1.25	1860	104.7	0.95
1450	122	1.45	1660	95.7	1	1870	106.3	0.7
1460	117.7	1.45	1670	98	0.8	1880	105.3	0.6
1470	125.3	1.3	1680	105	0.66	1890	106.3	1
1480	134.7	1.27	1690	112.7	0.6	1900	106.3	1.6
1490	139	1.35	1700	120.7	0.6	1910	114	2
1500	130	1.3	1710	120.7	0.96	1920	111.7	2.44
1510	114.7	1.38	1720	124	1.8	1930	112.7	3.2
1520	110.3	1.5	1730	129	2.56	1940	102.7	3.1
1530	109.3	1.76	1740	128	2.24	1950	100.7	2.5
1540	112	1.36	1750	126	1.6	1960		2.1
1550	102	1.2	1760	121.3	1.36			

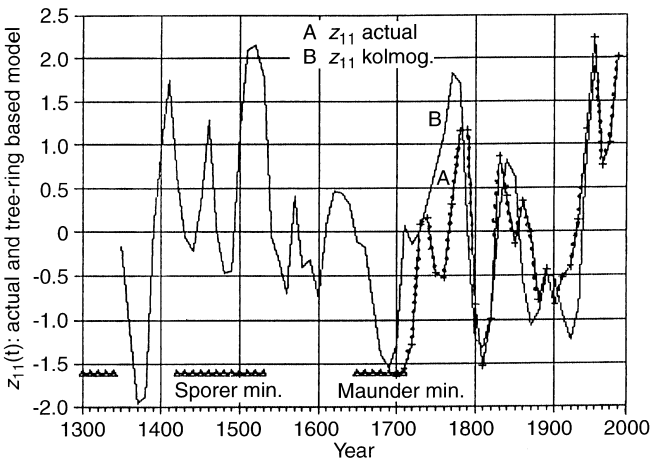

Fig. 23. Tree-rings and past solar activity

Of particular interest is the fact that the lowest part of $TR(t)$ coincides with the Maunder Minimum (1645–1715), during which sunspot activity had ceased to exist. Following these observations, it becomes tempting to reverse the roles of $TR(t)$ and $z_{11}(t)$ and apply the Kolmogorov algorithm to the case in order to provide a glimpse into $z_{11}(t)$'s past. The algorithm produces the transfer function:

i (years)	$w(i)$	i (years)	$w(i)$
−90	−0.015	−40	+0.141
−80	+0.207	−30	+0.282
−70	−0.170	−20	+0.070
−60	−0.227	−10	+0.192
−50	+0.116	0	−0.327 ,

(35)

with the final outcome given in Fig. 23 diagramming the long-term course of $z_{11}(t)$ before the invention of the telescope. The most important finding about this connection, however, is that the time course of its terrestrial partner *leads* the solar partner, which of course means that a factor other than $z_{11}(t)$ – either solar or extra-solar – is operative in this case.

7 Conclusions

A diversified group of terrestrial phenomena has been examined in the context of a possible match between their historical record and the record of a surrogate of long-term solar activity. For lack of scientific knowledge on any causality connecting the two, only the morphology of the possible liaison was extracted. Based on both the rationale and the actual results of this analysis, it can be stated that:

1. In a number of important geophysical phenomena involving the earth's atmosphere and geosphere a solar-terrestrial connection does exist.
2. The proposed surrogate z_{11} of long-term solar activity does make for a quantitative intermediary of solar-terrestrial connections.
3. The mathematical modeling of z_{11} itself does provide a tool of projecting geophysical processes.
4. The Kolmogorov algorithm of time-signal analysis can diagram the time course of geophysical processes, though their physical mechanism is presently unknown, and can effect their projection.
5. In all the connection cases examined, incommensurate frequencies do appear, pointing to process nonlinearity.
6. Most always one of these frequencies is that of the magnetic polarity of the sunspot cycle, i.e., 22 years.
7. Finally, such anthropogenic factors as CO_2 and SO_2 do exert important forcing upon climate.

For all these occurrences, although 'connection' does not necessarily imply causality, it does indicate synchronization (Friis-Christensen and Lassen, 1991), the degree of which can be judged by the degree of similarity between the autocorrelation function $z_{11} * z_{11}$ of the solar member z_{11}, and the cross-correlation function $X_{11} * z_{11}$ between solar z_{11} and terrestrial X_{11}. By the same token, lack of such coherence renders a connection between X_{11} and z_{11} doubtful.

Finally, the tree-ring case raises the possibility of a causal factor external to the known solar system and leading the postulated solar surrogate $z_{11}(t)$ itself.

We would like to end this essay by invoking the observations of D.E. Walker of the Hawaii Institute of Geophysics and Planetology, who begins a recent paper of his as follows:

> In 1988, evidence showed a connection between the five extreme lows of the Southern Oscillation Index from 1964 through 1987 and episodic seismic activity along the East Pacific Rise from 20°S to 40°S, an area that contains one of the earth's most rapidly spreading ridge systems. Observed coincidences are often the basis for discovery, and reviewing the available data leads us to note several. Two distinct phenomena – El Ninos and earthquake swarms – seem to occur almost simultaneously in spite of their irregular recurrence rates and durations. (Walker, 1995).

As a footnote, it should be pointed out that the purpose of the numerous Appendices included in this essay is the hope that other investigators specializing in particular topics would use them either to extend or refute the thesis advocated in this study.

Appendix 1a Southern Oscillation Index (seasonal)

year	win DJF	sum JJA	spr MAM	aut SON	year	win DJF	sum JJA	spr MAM	aut SON	year	win DJF	sum JJA	spr MAM	aut SON
1860	0.69	0.19	0.26	−0.0	1898	0.3	0.18	1.58	0.65	1936	−0.4	0.3	−0.1	0.05
1861	0.83	1.42	1.17	0.15	1899	1.14	−1.6	−0.1	−1.5	1937	0.93	0.01	0.58	0.31
1862	1.17	0.98	1.11	1.64	1900	−1.2	−0.7	−1.1	−0.2	1938	1.1	1.12	1.12	0.83
1863	1.91	1.33	1.86	0.35	1901	−0.5	−0.6	−0.4	−0.3	1939	1.03	−0.1	0.52	−0.6
1864	−0.0	−1.2	−1.0	−0.6	1902	−0.0	−2.0	−1.1	−1.2	1940	−0.6	−2	−1.2	−1.9
1865	−1.2	−0.6	−0.0	0.08	1903	−1.5	0.64	−0.9	0.83	1941	−1.0	−1.4	−1.7	−1.2
1866	−0.1	−0.3	−0.0	−0.0	1904	0.76	−0.6	0.77	−0.8	1942	−0.6	1.1	−0.2	0.81
1867	−1.3	0.69	−0.1	0.48	1905	−2.2	−1.0	−2.0	−0.5	1943	0.6	0.26	0.06	0.32
1868	−1.8	−1.9	−1.5	−1.4	1906	−1.4	0.72	−0.5	0.33	1944	−0.4	−0.4	−0.4	0.12
1869	−0.1	−0.1	−1.1	0.41	1907	0.32	−0.3	−0.1	−0.3	1945	1.44	−0.1	0.42	0.19
1870	1.43	0.76	1.17	1	1908	−0.1	−0.0	0.62	0.65	1946	0.12	−0.3	0.07	−0.3
1871	0.76	0.37	0.2	0.4	1909	0.42	1.68	0.86	0.95	1947	1.07	0.28	0.15	0.86
1872	0.88	1.39	0.84	1.42	1910	0.91	1.21	1.84	1.04	1948	0.14	0.28	0.17	0.5
1873	1.99	0.92	0.52	−0.6	1911	0.84	−1	−0.9	−1.0	1949	−0.0	0.53	−0.0	1.16
1874	−1.8	1.26	0.34	1.41	1912	−0.8	0.27	−0.9	−0.0	1950	1.02	1.3	1.05	0.74
1875	0.31	0.25	0.93	0.24	1913	−0.1	−0.8	0.47	−1.0	1951	0.09	−0.1	0.59	0.09
1876	0.71	−1.3	0.29	−1.5	1914	−0.1	−1.6	−1.2	−1.9	1952	−0.0	0.7	0.56	0.19
1877	−1.8	−4.1	−2.0	−3.4	1915	−1.0	1.3	−1.0	1.09	1953	0.45	−0.1	0.3	0.22
1878	−1.3	0.58	−1.2	1.95	1916	0.76	2.85	1.32	2.38	1954	−0.1	0.68	0.56	0.74
1879	0.92	1.05	0.24	0.46	1917	2.33	2.64	1.89	2.45	1955	0.39	1.5	2.1	2.13
1880	1.47	−0.8	−0.3	−0.9	1918	0.99	−0.9	−0.5	−1.0	1956	1.47	2.14	1.75	1.03
1881	−1.6	−1.0	−1.6	−0.2	1919	−0.9	−0.3	−1.0	−0.2	1957	0.45	−0.7	−0.4	−0.9
1882	0.62	1.23	0.65	0.52	1920	−0.5	0.93	0.18	0.23	1958	−1.0	0.26	−0.6	0.51
1883	0.29	0.3	0.81	−0.2	1921	1.34	1.26	1.31	0.22	1959	−0.2	−0.1	−0.1	0.34
1884	−0.6	−0.3	−0.3	−0.3	1922	0.4	0.55	0.76	0.58	1960	0.8	0.77	0.52	0.67
1885	−0.8	−1.4	−0.1	−1	1923	0.78	0.58	0.43	−0.6	1961	0.17	0.78	0.59	1.6
1886	−0.8	1.28	0.7	1.62	1924	−0.1	0.63	0.72	1.16	1962	1.3	1.2	1.44	0.74
1887	0.59	−0.1	0.45	−0.6	1925	0.6	−0.6	0.97	−1.3	1963	0.65	0.01	0.53	−0.9
1888	−0.8	−0.6	−0.9	−1.5	1926	−1.8	0.08	−1.6	0.63	1964	−1.1	1.12	0.28	0.62
1889	−1.4	1.18	−1.0	1.29	1927	0.72	0.04	0.9	−0.2	1965	−0.2	−1.5	−0.1	−0.7
1890	2.19	1.11	1.21	0.53	1928	−0.6	−0.0	0.43	0.5	1966	−0.8	−0.3	−0.3	0.32
1891	−0.3	−0.9	−0.8	−0.4	1929	0.2	−0.6	0.52	−0.3	1967	0.74	0.09	0.25	0.27
1892	0.09	0.93	1.54	1.64	1930	0.24	−1.3	−0.8	−1.0	1968	0.04	1.05	0.27	−0.5
1893	0.88	2.06	1	1.22	1931	−0.7	0.33	−0.7	0.59	1969	0.46	−0.4	−0.2	−0.6
1894	0.81	0.72	0.66	0.91	1932	−0.3	0.41	−0.2	0.56	1970	−0.2	0.9	−0.0	1.34
1895	−0.0	−0.1	0.66	0.02	1933	0.53	0.81	0.6	1.26	1971	1.6	0.83	1.63	1.64
1896	−0.0	−0.8	0.24	−1.4	1934	1.48	−0.2	0.53	0.07	1972	1.06	−2.2	−0.0	−1.2
1897	−0.6	0.11	−0.1	0.72	1935	0.11	−0.1	0.2	0.06	1973	−0.7	1.04	0.6	1.57
										1974	2.16	1.3	1.71	1.11

Appendix 1b Southern Oscillation Index (long-term)

year	O (*t*) spraut	O_{11} (*t*) spraut 11	year	O (*t*) spraut	O_{11} (*t*) spraut 11	year	O (*t*) spraut	O_{11} (*t*) spraut 11	year	O (*t*) spraut	O_{11} (*t*) spraut 11
1860	0.1	–	1893	1.11	0.21	1926	−0.52	0.4	1959	0.115	0.54
1861	0.66	–	1894	0.785	0.25	1927	0.31	0.26	1960	0.595	0.55
1862	1.375	–	1895	0.34	0.32	1928	0.465	0.1	1961	1.095	0.56
1863	1.105	–	1896	−0.62	0.31	1929	0.105	0.18	1962	1.09	0.63
1864	−0.82	–	1897	0.3	0.23	1930	−0.97	0.15	1963	−0.22	0.58
1865	0.025	–	1898	1.115	0.34	1931	−0.08	0.13	1964	0.45	0.6
1866	−0.05	–	1899	−0.87	0.37	1932	0.145	0.07	1965	−0.43	0.5
1867	0.165	–	1900	−0.69	0.3	1933	0.93	0.09	1966	−0.01	0.3
1868	−1.52	–	1901	−0.37	0.19	1934	0.3	0.13	1967	0.26	0.2
1869	−0.37	–	1902	−1.2	0.13	1935	0.13	0.06	1968	−0.12	0.25
1870	1.085	0.16	1903	−0.07	−0.02	1936	−0.05	0.07	1969	−0.41	0.22
1871	0.3	0.18	1904	−0.05	−0.12	1937	0.445	0.16	1970	0.65	0.27
1872	1.13	0.22	1905	−1.29	−0.31	1938	0.975	0.22	1971	1.635	0.36
1873	−0.05	0.09	1906	−0.08	−0.35	1939	−0.07	0.17	1972	−0.65	0.2
1874	0.875	0.07	1907	−0.24	−0.32	1940	−1.58	0.01	1973	1.085	0.2
1875	0.585	0.2	1908	0.635	−0.29	1941	−1.51	−0.03	1975	1.385	0.44
1876	−0.60	0.14	1909	0.905	−0.3	1942	0.275	0	1976	1.035	0.57
1877	−2.71	−0.1	1910	1.44	−0.09	1943	0.19	0	1977	0.235	0.59
1878	0.345	−0.09	1911	−1	−0.12	1944	−0.15	−0.1	1978	0.235	0.59

Appendix 1b (*Contd.*)

year	O (t) spraut	O_{11} (t) spraut 11	year	O (t) spraut	O_{11} (t) spraut 11	year	O (t) spraut	O_{11} (t) spraut 11	year	O (t) spraut	O_{11} (t) spraut 11
1879	0.35	0.09	1912	−0.50	−0.13	1945	0.305	−0.1	1979	0.585	0.65
1880	−0.64	0.06	1913	−0.29	−0.05	1946	−0.12	−0.12	1980	0.485	0.74
1881	−0.97	−0.13	1914	−1.58	−0.19	1947	0.505	−0.07	1981	0.61	0.73
1882	0.585	−0.1	1915	0	−0.18	1948	0.335	−0.08	1982	−0.06	0.58
1883	0.305	−0.18	1916	1.85	0.1	1949	0.56	−0.12	1983	−0.21	0.62
1884	−0.38	−0.21	1917	2.17	0.31	1950	0.895	−0.03	1984	0.66	0.58
1885	−0.57	−0.34	1918	−0.79	0.26	1951	0.34	0.15	1985	0.81	0.52
1886	1.16	−0.29	1919	−0.64	0.14	1952	0.375	0.32	1986	0.435	0.44
1887	−0.08	−0.24	1920	0.205	0.08	1953	0.26	0.32	1987	0.06	0.35
1888	−1.20	−0.1	1921	0.765	0.02	1954	0.65	0.36	1988	1.085	0.43
1889	0.135	−0.12	1922	0.67	0.17	1955	2.115	0.57	1989	1.035	0.5
1890	0.87	−0.07	1923	−0.13	0.2	1956	1.39	0.66	1990	0.435	0.48
1891	−0.64	−0.07	1924	0.94	0.31	1957	−0.69	0.61	1991	0.01	0.44
1892	1.59	0.16	1925	−0.17	0.44	1958	−0.04	0.56	1992	−0.31	0.36

Appendix 2 Carbon dioxide CO_2

year	CO_2	year	CO_2	year	CO_2	year	CO_2	year	CO_2
1800	279.3	1838	285.8	1876	292.9	1914	300	1952	312.0
1801	279.4	1839	286	1877	293.1	1915	300.3	1953	312.4
1802	279.5	1840	286.1	1878	293.4	1916	300.6	1954	312.7
1803	279.7	1841	286.2	1879	293.6	1917	301	1955	313.1
1804	279.8	1842	286.4	1880	293.8	1918	301.3	1956	313.4
1805	280	1843	286.5	1881	294.0	1919	302.6	1957	313.8
1806	280.2	1844	286.7	1882	294.3	1920	302	1958	314.2
1807	280.4	1845	286.8	1883	294.5	1921	302.3	1959	314.7
1808	280.6	1846	287	1884	294.7	1922	302.6	1960	315.2
1809	280.8	1847	287.1	1885	294.9	1923	303	1961	315.8
1810	281	1848	287.2	1886	295.2	1924	303.3	1962	316.3
1811	281.2	1849	287.4	1887	295.4	1925	303.6	1963	316.9
1812	281.4	1850	287.5	1888	295.6	1926	304	1964	317.4
1813	281.6	1851	287.7	1889	295.8	1927	304.3	1965	318
1814	281.8	1852	287.8	1890	296.1	1928	304.6	1966	319.2
1815	282	1853	288	1891	296.3	1929	305	1967	320.5
1816	282.2	1854	288.2	1892	296.5	1930	305.3	1968	321.7
1817	282.4	1855	288.4	1893	296.7	1931	305.6	1969	323
1818	282.6	1856	288.6	1894	297	1932	306	1970	324.2
1819	282.8	1857	288.8	1895	297.1	1933	306.2	1971	325.5
1820	283	1858	289.0	1896	297.3	1934	306.5	1972	326.7
1821	283.2	1859	289.2	1897	297.4	1935	306.8	1973	328
1822	283.4	1860	289.5	1898	297.6	1936	307.1	1974	329.2
1823	283.6	1861	289.7	1899	297.7	1937	307.4	1975	330.5
1824	283.8	1862	289.9	1900	297.9	1938	307.7	1976	331.7
1825	284	1863	290.1	1901	298.0	1939	308.0	1977	333
1826	284.1	1864	290.3	1902	298.2	1940	308.3	1978	334.2
1827	284.2	1865	290.5	1903	298.3	1941	308.6	1979	335.5
1828	284.4	1866	290.7	1904	298.5	1942	308.9	1980	336.7
1829	284.5	1867	291.0	1905	298.6	1943	309.2	1981	338
1830	284.7	1868	291.2	1906	298.8	1944	309.5	1982	339.2
1831	284.8	1869	291.4	1907	298.9	1945	309.8	1983	340.5
1832	285	1870	291.6	1908	299.1	1946	310.1	1984	341.7
1833	285.1	1871	291.8	1909	299.2	1947	310.4	1985	343
1834	285.2	1872	292.0	1910	299.4	1948	310.7	1986	344.2
1835	285.4	1873	292.3	1911	299.5	1949	311	1987	345.5
1836	285.5	1874	292.5	1912	299.7	1950	311.3	1988	346.7
1837	285.7	1875	292.7	1913	299.8	1951	311.7	1989	348
								1990	349.2

Appendix 3 Sulphur dioxide SO_2

year	SO_2	year	SO_2	year	SO_2	year	SO_2	year	SO_2
1800	1.4	1838	1.62	1876	5.2	1914	24.8	1952	43.4
1801	1.40	1839	1.63	1877	5.45	1915	25.1	1953	44.3
1802	1.40	1840	1.65	1878	5.7	1916	25.4	1954	45.0
1803	1.40	1841	1.67	1879	5.95	1917	25.7	1955	45.6
1804	1.40	1842	1.7	1880	6.2	1918	26.0	1956	46.1
1805	1.41	1843	1.72	1881	6.68	1919	26.3	1957	46.6
1806	1.41	1844	1.75	1882	7.16	1920	28	1958	50
1807	1.41	1845	1.77	1883	7.64	1921	28.3	1959	51.3
1808	1.41	1846	1.8	1884	8.12	1922	28.6	1960	52.7
1809	1.41	1847	1.82	1885	8.6	1923	28.9	1961	54.1
1810	1.42	1848	1.85	1886	9.08	1924	29.2	1962	55.5
1811	1.42	1849	1.87	1887	9.56	1925	29.5	1963	56.9
1812	1.42	1850	1.9	1888	10.0	1926	29.8	1964	58.3
1813	1.42	1851	1.96	1889	10.5	1927	30.1	1965	59.7
1814	1.43	1852	2.02	1890	11	1928	30.4	1966	61.1
1815	1.43	1853	2.08	1891	11.4	1929	30.7	1967	62.5
1816	1.43	1854	2.14	1892	11.8	1930	31	1968	63.4
1817	1.44	1855	2.2	1893	12.2	1931	31.6	1969	64.3
1818	1.44	1856	2.26	1894	12.7	1932	32.2	1970	65.2
1819	1.44	1857	2.32	1895	13.1	1933	32.8	1971	66.1
1820	1.45	1858	2.38	1896	13.5	1934	33.4	1972	67.0
1821	1.45	1859	2.44	1897	14.0	1935	34	1973	68
1822	1.46	1860	2.5	1898	14.4	1936	34.6	1974	69.5
1823	1.46	1861	2.62	1899	14.8	1937	35.2	1975	71
1824	1.47	1862	2.74	1900	15.3	1938	35.8	1976	72.5
1825	1.48	1863	2.86	1901	16.1	1939	36.4	1977	74
1826	1.48	1864	2.98	1902	16.9	1940	37	1978	75
1827	1.49	1865	3.1	1903	17.7	1941	37.4	1979	76
1828	1.49	1866	3.22	1904	18.5	1942	37.9	1980	77
1829	1.50	1867	3.34	1905	19.4	1943	38.3	1981	78
1830	1.51	1868	3.46	1906	20.2	1944	38.8	1982	79
1831	1.52	1869	3.58	1907	21.0	1945	39.2	1983	80
1832	1.53	1870	3.7	1908	21.8	1946	39.7	1984	81
1833	1.55	1871	3.95	1909	22.6	1947	40.1	1985	82.3
1834	1.56	1872	4.2	1910	23.5	1948	40.6	1986	83.6
1835	1.58	1873	4.45	1911	23.9	1949	41.0	1987	85
1836	1.59	1874	4.7	1912	24.2	1950	41.5	1988	86.3
1837	1.60	1875	4.95	1913	24.5	1951	42.5	1989	87.6

Appendix 4 Northern hemisphere temperature

year	temp.	year	temp.	year	temp.	year	temp.	year	temp.
1855	–	1882	−0.16	1909	−0.36	1936	−0.02	1963	0.09
1856	−0.2	1883	−0.23	1910	−0.31	1937	0.1	1964	−0.2
1857	−0.3	1884	−0.12	1911	−0.36	1938	0.21	1965	−0.14
1858	−0.22	1885	−0.26	1912	−0.3	1939	0.09	1966	−0.04
1859	−0.06	1886	−0.2	1913	−0.29	1940	0.14	1967	−0.03
1860	−0.27	1887	−0.27	1914	−0.08	1941	0.21	1968	−0.05
1861	−0.29	1888	−0.18	1915	0.04	1942	0.09	1969	0.08
1862	−0.41	1889	−0.1	1916	−0.25	1943	0.06	1970	0.01
1863	−0.14	1890	−0.25	1917	−0.38	1944	0.24	1971	−0.15
1864	−0.3	1891	−0.23	1918	−0.28	1945	0.09	1972	−0.04
1865	−0.1	1892	−0.28	1919	−0.21	1946	0	1973	0.014
1866	−0.06	1893	−0.32	1920	−0.14	1947	0.01	1974	−0.14
1867	−0.15	1894	−0.23	1921	−0.12	1948	−0.02	1975	−0.07
1868	−0.09	1895	−0.25	1922	−0.21	1949	−0.04	1976	−0.17
1869	−0.11	1896	−0.05	1923	−0.17	1950	−0.14	1977	0.1
1870	−0.18	1897	−0.03	1924	−0.21	1951	0	1978	0.01
1871	−0.24	1898	−0.2	1925	−0.1	1952	0.08	1979	0.11
1872	−0.1	1899	−0.07	1926	0.06	1953	0.15	1980	0.16
1873	−0.21	1900	0.01	1927	−0.07	1954	−0.09	1981	0.21
1874	−0.24	1901	−0.02	1928	−0.07	1955	−0.11	1982	0.12
1875	−0.33	1902	−0.18	1929	−0.25	1956	−0.21	1983	0.3
1876	−0.29	1903	−0.27	1930	−0.05	1957	0.09	1984	0.1
1877	0.04	1904	−0.34	1931	0.03	1958	0.16	1985	0.07
1878	0.17	1905	−0.25	1932	−0.02	1959	0.09	1986	0.15
1879	−0.19	1906	−0.18	1933	−0.15	1960	0.06	1987	0.3
1880	−0.18	1907	−0.41	1934	−0.03	1961	0.07	1988	0.31
1881	−0.19	1908	−0.4	1935	−0.05	1962	0.08	1989	0.23

Appendix 5 California earthquakes

year	$Q(t)$	q_{max}	year	$Q(t)$	q_{max}	year	$Q(t)$	q_{max}	year	$Q(t)$	q_{max}
1902	22.5	8	1924	6	6	1946	20	8	1968	51	7
1903	27	7	1925	14.5	8.5	1947	25	7	1969	38.5	7.5
1904	0		1926	27	8	1948	27	7	1970	31	7
1905	0		1927	56.5	9.5	1949	37	7	1971	30	11
1906	33	8	1928	12	7	1950	33	8	1972	18	6
1907	13	7	1929	14	7	1951	81	7	1973	13	7
1908	14	7	1930	62	8	1952	103	11	1974	24	6
1909	22.5	8	1931	12	6	1953	38.5	7.5	1975	113	8
1910	13	7	1932	24	10	1954	109	10	1976	54	6
1911	13.5	7.5	1933	29	9	1955	55	7	1977	55	7
1912	6.5	6.5	1934	29.5	8.5	1956	54	6	1978	49	7
1913	0		1935	0		1957	32	7	1979	78	9
1914	20	7	1936	6	6	1958	42	6	1980	59	7
1915	39	10	1937	13.5	7	1959	73	7	1981	43	7
1916	33	7	1938	24.5	6	1960	12	6	1982	18	6
1917	12.5	6.5	1939	25	7	1961	44	7	1983	56	8
1918	40	9	1940	28.5	10	1962	37	7	1984	22	8
1919	20	7	1941	53.5	8	1963	49	7	1985	12	9
1920	21	8	1942	13	7	1964	25	7	1986	39	7
1921	15	9	1943	13	7	1965	49	7	1987	34	7
1922	6	6	1944	12	6	1966	56	7	1988	24	6
1923	28.5	7.5	1945	24	6	1967	48	6	1989	46	9

Appendix 6 Active volcanos

year	$v(t)$	year	$v(t)$	year	$v(t)$	year	$v(t)$	year	$v(t)$	year	$v(t)$
1790	40	1823	25	1856	30	1889	33	1922	40	1955	56
1791	24	1824	20	1857	24	1890	36	1923	41	1956	51
1792	24	1825	31	1858	23	1891	27	1924	44	1957	56
1793	21	1826	23	1859	26	1892	32	1925	38	1958	47
1794	14	1827	26	1860	31	1893	33	1926	44	1959	50
1795	12	1828	29	1861	21	1894	35	1927	44	1960	47
1796	17	1829	32	1862	19	1895	32	1928	51	1961	50
1797	19	1830	39	1863	26	1896	31	1929	53	1962	45
1798	17	1831	24	1864	29	1897	34	1930	37	1963	60
1799	18	1832	21	1865	33	1898	27	1931	37	1964	56
1800	24	1833	24	1866	22	1899	31	1932	35	1965	55
1801	16	1834	21	1867	31	1900	31	1933	40	1966	65
1802	18	1835	29	1868	31	1901	28	1934	38	1967	65
1803	18	1836	14	1869	33	1902	42	1935	39	1968	55
1804	19	1837	18	1870	31	1903	34	1936	38	1969	49
1805	18	1838	29	1871	28	1904	46	1937	36	1970	53
1806	19	1839	18	1872	28	1905	38	1938	42	1971	61
1807	20	1840	17	1873	31	1906	46	1939	47	1972	61
1808	19	1841	14	1874	30	1907	52	1940	43	1973	75
1809	16	1842	22	1875	28	1908	30	1941	29	1974	72
1810	16	1843	30	1876	26	1909	37	1942	29	1975	59
1811	19	1844	30	1877	33	1910	36	1943	32	1976	59
1812	27	1845	29	1878	31	1911	37	1944	37	1977	67
1813	20	1846	34	1879	25	1912	34	1945	36	1978	53
1814	23	1847	24	1880	32	1913	36	1946	42	1979	55
1815	18	1848	25	1881	26	1914	39	1947	43	1980	65
1816	14	1849	23	1882	25	1915	36	1948	39	1981	55
1817	22	1850	28	1883	44	1916	25	1949	49	1982	64
1818	19	1851	16	1884	33	1917	36	1950	47	1983	51
1819	22	1852	39	1885	37	1918	28	1951	66	1984	51
1820	19	1853	24	1886	35	1919	29	1952	59	1985	58
1821	24	1854	29	1887	35	1920	31	1953	63		
1822	25	1855	22	1888	33	1921	44	1954	50		

Acknowledgements. The Editor-in-Chief thanks two referees for their help in evaluating this paper.

References

Andersen, C. P., S. B. McLaughlin, and W. K. Roy, A comparison of seasonal patterns of photosynthate production and use in

branches of red spruce saplings at two elevations, *Can. J. For. Res.*, **21,** 455–461, 1991.
Anderson, D. L. T., and J. P. McRay, Slowly propagating disturbances in a coupled ocean-atmosphere model, *J. Atmos. Sci.,* **42,** 615–628, 1985.
Angell, J. K., and J. Korshover, Surface temperature changes following six major volcanic episodes between 1780 and 1980, *J. Clim. Appl. Meteorol.*, **24,** 937–951, 1985.
Ayres, R. U., and J. Walter, The greenhouse effect: damages, costs and abatement, *Environ. Resour. Econ.*, 1, 237–270, 1991
Cane, M. A., S. E. Zebiak, and S. C. Dolan, Experimental forecast of El Nino, *Nature*, **321,** 827–831, 1986.
Charlson, R. J., S. E. Charlson, S. E. Schartz, J. M. Hales, R. D. Cess, J. A. Coakley Jr, J. E. Hansen, and D. J. Hoafmann, Climate forcing by anthropogenic aerosols, *Science*, **255,** 423–430, 1992.
Diamantides, N. D., Long-term solar activity and terrestrial connections. Part I: theory, *Ann. Geophysicae*, in press, 1998.
Eddy, J. A, The Maunder Minimum, *Science*, **192,** 1189–1202, 1976.
Enfield, B. F. and S. L. Cid, Low frequency changes in El Nino-Southern Oscillation, *J. Clim.*, **4,** 1137–1145, 1991.
Francey, R. J. and G. D. Farquhar, An explanation of $^{13}C/^{12}C$ variations in tree rings, *Nature*, **297,** 28–31, 1982.
Friis-Christensen, E. and K. Lassen, Length of the solar cycle: an indicator of solar activity closely associated with climate, *Science*, **254,** 698–700, 1991.
Gribbin, J. R., and S. H. Plagemann, *The Jupiter effect*, Walker, New York, 1974.
Hollstein, E, Jahrringchronologische Datierung von Eichenholzer-uchne Waldkante (westdeutsch Eichenchronologie) *Bonn. Jahrbuch.*, **165,** 1–27, 1965.
Jones, P. D., T. M. L. Wigley, and P. B. Wright, Global temperature variations between 1861 and 1984, *Nature* **322,** 430–433, 1986.
Kellogg, W. W., Aerosols and global warming, *Science*, **256,** 598–599, 1992.
Kerr, R. A, Could the Sun be warming the climate? *Science*, **254,** 652–653, 1991.
Lamb, H. H., *Climate: past, present, and future*, vol. 1, Methuen, London, 1973.
Legrand, J. P., and P. A. Simon, Solar cycle and geomagnetic activity, review for geophysicists. I The contribution to geomagnetic activity of shock waves and of the solar wind, *Ann. Geophysicae*, **7,** 565–578, 1989.
Lelieveld, J., and J. Heintzenberg, Sulfate cooling effect on climate trough in-cloud oxidation of anthropogenic SO_2, *Science*, **258,** 117–119, 1992.
Libby, L. M., and L. J. Pandolfi, Temperature dependence of isotope ratios in tree rings, *Proc. Nat. Acad. Sci., USA*, vol. **71,** 2482–2486, 1974.
Lomnitz, C., *Fundamentals of earthquake prediction*, Wiley, New York, 1994.
McClelland, L., T. Simkin, M. Summers, E. Nielsen, and T. Stein (eds), *Global volcanism 1975–1985*, Prentice Hall, Englewood Cliffs, NJ, 1989.
McLaughlin, S. B., and D. J. Downing, Interactive effects of ambient ozone and climate measured on growth of mature forest trees. *Nature*, **374,** 252–254, 1995.
McLaughlin, S. B., and M. J. Tjoelker, Growth and physiological changes in spruce saplings associated with acid deposition at high altitudes in the southern Appalachians, *For. Ecol. Manage.*, **51,** 43–51, 1992.
McLaughlin, S. B., and M. J. Tjoelker, Acid deposition alters red spruce physiology, *Can. J. For. Res.*, **23,** 380–386, 1993.
McLaughlin, S. B., P. A. Layton, M. B. Adams, M. B. Adams, N. T. Edwards, and P. J. Hanson, Growth responses of 53 open-pollinated loblolly-pine families to ozone and acid rain, *J. Environ. Quality*, **23,** 247–257, 1994.
Mendoza, B., R. Perez-Enriquez, and M. Alvarez-Madrigal, Analysis of solar activity conditions during periods of El Nino events, *Ann. Geophys.*, **9,** 50–54, 1991.
Moller, D., Estimation of the global manmade sulphur emission, *Atmos. Environ.*, **18,** 19–27, 1984.
Monastersky, R., The long view of weather, *Sci. News*, **144,** 328–330, 1993.
Naftel, A., E. Moor, and H. Oeschger, Evidence from polar ice cores for the increase in atmospheric CO_2 in the last two centuries, *Nature*, **315,** 45–47, 1985.
National Weather Service, *Climate diagnostics bulletin,* Climate Analysis Center, Washington DC, 1992.
Oechel, W. C., S. J. Hastings, G. Vourliotis, and M. Jenkins, Recent change of Arctic Tundra ecosystems from a net carbon dioxide sink to a source, *Nature*, **361,** 520–523, 1993.
Pacheco, J. F., C. H. Schelz, and L. R. Sykes, Changes in frequency-size relationship from small to large earthquakes, *Nature*, **365,** 71–73, 1992.
Phillander, G., *El Nino, La Nina, and the Southern Oscillation*. Academic Press, New York, 1992.
Plantico, M. S., T. R. Karl, and J. Gavin, Is recent climate change across the United States related to rising changes to the levels of atmospheric greenhouse gasses?, *J. of Geoph. Res.*, **95,** 16.617–16.637, 1990
Ping, C., J. I. Link, and L. J. Hong, A decadal climate variation in the tropical Atlantic Ocean from thermodynamic air-sea interactions, *Nature*, **385,** 516–518, 1997.
Prentice, K. C., and I. Y. Funk, The sensitivity of terrestrial carbon storage to climate change, *Nature*, **346,** 48–50, 1995.
Quinn, W. H., T. V. Neal, and S. Antunes-Mayolo, El Nino occurrences over the past four-and-a-half centuries, *J. Geophys. Res.*, **92,** 414–449, 1987.
Simkin, T., Distant effects of volcanism – how big and how often, *Science*, **264,** 913–914, 1994.
Simkin, T., L. Seibert, L. McClelland, D. Bridge, C. Newhall and J. H. Latter, *Volcanoes of the world*, Hutchinson Ross, Stroudsburg, PA, 1981.
Simon, P. A., and J. P. Legrand, Solar cycle and geomagnetic activity for geophysicists "II The solar sources of geomagnetic activity and their links with sunspot cycle activity, *Annal. Geophys.*, **7,** 579–594, 1989.
Simpson, J. F, Solar activity as a triggering mechanism, *Earth Planet. Sci. Lett.*, **3,** 417–425, 1967.
Singh, S., Geomagnetic activity and microearthquakes, *Bull. Seismol. Soc Am.*, **68,** 1533–1535, 1976.
Smith, T. M., and H. H. Shugart, The transient response of terrestrial carbon storage to a perturbed climate, *Nature*, **361,** 523–526, 1993.
Sytinski, A. D., Recent tectinic movements as one of the manifestations of solar activity, *Geomagn. Aeron.* **3,** 120–126, 1963.
U.S. Government Reports (1) **Coffman, J. L. and C. A. von Hakein** (Eds), *Earthquake history of the United States*, Pub. 41-1, (2) **Stover, C.** (Ed.) *United States earthquakes 1981*, US Geol Surv Special Pub. (3) **United States Earthquakes 1981**, **1982**, **1983**, **1984**, U.S. Geological Survey Special Publications, Bulletins 1655, 1698, 1882. (4) **Stover, C. W, and J.L. Coffman** 1993, *Seismicity of the United States, 1569-1989* (Revised), U.S. Geological Survey Paper 1527 U.S. Government Printing Office, Washington, DC.
Walker, D. A., More evidence indicates link between El Ninos and seismicity, *EOS Trans.*, **76** (4), 33–36, 1995.
Whalen, M., D. Allen, and B. Deck, Initial measurements of CO_2 Concentrations (1530 to 1940) in air occluded in the GISP 2 ice core from central Greenland, *Geoph. Res. Letters*, **18**, 1457–1460, 1991.
Wigley, T. M. E., and S. C. B. Raper, Implications for climate and sea-level of revised IPCC emissions senarios, *Nature*, **357,** 293–300, 1992.
Wright, P. B., The Southern Oscillation: patterns and mechanisms of their teleconnections and persistence, *HIG.77.13*, Hawaii Institute of Geophysics, University of Hawaii, 1977.
Wright, P. B., An index of the southern Oscillation, *Clim. Res. Unit Rep.* CRU **RP4,** 1995.
Zielinski, G. A., P. A Mayewski, L. D. Mmeeker, S. Whitlow, M. S. Twickler, M. Morison, D. A. Meese, A. J. Gow, and R. B. Alley, Record of volcanism since 7000 B.C. from the GISP2 Greenland ice core and implications for the volcano-climate system, *Science*, **264,** 948–952, 1994.